applied sciences

MDPI

Article

Damage Localization in Thin Plates Using EMI Signals from a Piezoelectric Array with Regional RMSD Averaging and Multiplexed Parallel Acquisition

Lijun Yang and Wei Yan *

School of Civil Engineering and Future Cities, Ningbo University, Ningbo 315211, China; ylj9909@126.com
* Correspondence: yanwei@nbu.edu.cn; Tel.: +86-574-87609513; Fax: +86-574-87600355

Abstract

This paper proposes an improved damage localization method for thin steel plates, which is based on electro-mechanical impedance (EMI) signals acquired by a distributed piezoelectric sensor array. A finite element model of the thin steel plate with surface-bonded piezoelectric patches was established in ANSYS, and the accuracy of the constructed model was validated through comparison with analytical solutions. Conductance signals under intact and damaged structural conditions were extracted within the frequency range of 30–40 kHz, and the RMSD damage index was computed following Z-score standardization. A regional statistical approach was proposed in this work, which enables accurate identification of damaged regions by averaging the Root Mean Square Deviation (RMSD) values of the four piezoelectric patches surrounding each subdivided sub-region. Experimental tests were further conducted on a thin steel plate specimen to verify the effectiveness of the proposed method. In addition, a multiplexed parallel acquisition scheme was developed to shorten the total test duration while guaranteeing the reliability of the damage identification performance. Experimental results demonstrate that the proposed approach achieves effective damage localization for thin steel plates, and provides a promising technical solution for high-efficiency structural health monitoring of large-scale plate-type engineering structures.

Keywords: electro-mechanical impedance (EMI); piezoelectric array; Root Mean Square Deviation (RMSD); damage localization; multiplexed parallel acquisition; finite element method (FEM)

1. Introduction

Owing to their outstanding strength, convenient construction and excellent environmental adaptability, steel structural members have been extensively employed as core load-bearing components in critical engineering fields, including bridges, industrial plants and offshore platforms. Among these components, steel plate elements are susceptible to multiple types of damage during long-term service, such as local buckling, corrosion-induced thickness reduction and initial cracking, which is attributable to their complex stress distribution, thin-walled geometrical characteristics and high sensitivity to local stress concentration. These damages generally originate at local sites, featuring small dimensions and concealed positions, which renders conventional visual inspection and traditional non-destructive testing (NDT) methods [1] unable to achieve timely damage detection. Delayed damage diagnosis will further trigger progressive degradation of the overall mechanical performance of steel structures, and may even ultimately result in catastrophic structural collapse.

Check for updates

Academic Editor: Marco Zucca

Received: 20 October 2026
Revised: 17 November 2026
Accepted: 26 November 2026
Published: 29 November 2026

Copyright: © 2026 by the authors. Licensee MDPI, Basel, Switzerland. This article is an open access article distributed under the terms and conditions of the Creative Commons Attribution (CC BY) license.

Structural Health Monitoring (SHM) is a robust monitoring technology that enables real-time perception of structural service conditions, quantitative damage assessment and remaining useful life prediction, and has emerged as a critical technical approach to guarantee the long-term safety and service reliability of in-service engineering structures. The electro-mechanical impedance (EMI) method is a crucial non-destructive detection technique in the field of SHM. Based on the electro-mechanical coupling effect between piezoelectric transducers and the host structure, the method infers changes in structural service status by measuring the variation in local mechanical impedance of the structure under high-frequency excitation [2]. This method possesses high sensitivity to local changes in structural stiffness and mass distribution, and is particularly applicable to the identification of minor damage and early-stage structural degradation, making it one of the key technical approaches for early damage diagnosis of steel structural members.

Currently, EMI technology has been widely applied in the health monitoring of various engineering structures. Naoum et al. [3] and Sapidis et al. [4] investigated the damage evolution process of fiber-reinforced concrete under cyclic loading, and verified the stability and sensitivity of EMI technology under complex loading conditions. Lee [5] employed the electro-mechanical impedance (EMI) technique to evaluate the setting time of concrete. By embedding piezoelectric sensors directly into concrete specimens and continuously tracking the variation in impedance responses, the identification of the initial setting and final setting processes of concrete was realized. Winklberger et al. [6] applied the EMI method to crack detection of metallic joints. Baral et al. [7] developed a temperature compensation method to mitigate the interference of environmental temperature variation on admittance signal characteristics. Sahm et al. [8] further revealed the coupling mechanism of temperature and preload on the electrical response output of piezoelectric sensors. From the perspective of sensor configuration design, Parida et al. [9] investigated the influence of the dimension and arrangement scheme of piezoelectric patches on the stability of monitoring results, and confirmed that sensor deployment has a significant impact on damage detection accuracy.

With the advancement of data-driven methodologies, machine learning techniques have been gradually introduced into the analysis of EMI signals [10–12]. Bansal et al. [10] achieved the prediction of material strength based on piezoelectric sensing data, and verified the application potential of data-driven methods in EMI-based damage monitoring technologies. To address the issues of data scarcity and measurement inefficiency in deep learning-based flexural performance assessment of reinforced concrete, Ai and Zhang [13] introduced a data augmentation strategy based on deep-convolutional admittance generative adversarial networks. Likewise, facing the challenge of training deep convolutional neural networks (CNNs) with limited EMI data for accurate damage detection under varying temperatures, Du et al. [14] devised a multitask CNN to recognize bolt loosening. Nevertheless, these methods have inherent limitations. For instance, artificial neural networks generally demand extensive training datasets (e.g., samples of both damaged and pristine states), whereas obtaining damaged data is often costly or difficult in real-world engineering scenarios. Furthermore, the opaque nature of artificial neural networks makes the decision-making process for damage identification hard to interpret [15]. All the aforementioned methods [3–14] were developed on the basis of the drive-point electro-mechanical impedance (EMI) technique. However, the conventional EMI technique depends on a single piezoelectric transducer for signal acquisition. Although this approach can confirm the occurrence of structural damage, it generally fails to provide sufficient spatial information to support effective damage localization [16].

In recent years, researchers have made attempts to break through the technical limitations of the conventional drive-point impedance method, and turned to explore the coupling response information among multiple piezoelectric sensors. Meher and Sunny [17]

integrated drive-point impedance and cross electro-mechanical impedance to achieve multi-damage identification. Their research findings indicated that cross characteristics can more effectively reflect the influence of damage on the propagation path of structural stress waves. In subsequent in-depth research, Meher and Sunny [18] applied the cross electro-mechanical impedance method to the interfacial debonding detection of composite structures, which significantly improved the accuracy of damage localization. Yang and Yan [16,19] utilized the cross electro-mechanical impedance technique for damage localization of bolted connections and steel beams. Their research revealed that the proposed method, which connects two piezoelectric patches in parallel, can effectively capture the local dynamic characteristics between the two sensors and identify the sensor interval containing damage, and exhibits excellent application prospects in the field of structural health monitoring. However, the application of existing cross electro-mechanical impedance technology requires not only measuring the drive-point conductance signature of each piezoelectric patch, but also conducting additional measurement on adjacent piezoelectric patch pairs to obtain group admittance, and finally deriving cross admittance through post-processing calculation [16–19]. Such a procedure inevitably leads to low testing efficiency and prolonged measurement time, especially when a large number of piezoelectric patches are deployed.

To address these issues, this paper proposed an improved damage localization method for thin steel plates based on EMI signals from a distributed piezoelectric sensor array [20–22]. A finite element model of the thin steel plate with bonded piezoelectric patches [23–25] was first established in ANSYS R19.2, and the simulated conductance spectra were compared with analytical solutions to verify the model accuracy. A Z-score standardization method [4] was then adopted to process the raw conductance data before calculating the RMSD damage index [26–31], which effectively mitigates the calculation deviations caused by the characteristic discrepancies among individual piezoelectric patches and environmental variations. On this basis, a regional statistical method was further proposed by averaging the RMSD values of the four piezoelectric patches surrounding each sub-region, which significantly improves the accuracy of damage localization and overcomes the insufficient positioning accuracy of single-patch-based indices. Furthermore, experimental measurements were conducted on a steel plate with a piezoelectric sensor array, and the experimental results were basically consistent with the numerical simulation results, verifying the effectiveness and feasibility of the proposed method. Finally, a multiplexed parallel acquisition scheme was developed by connecting the four piezoelectric patches within each monitoring sub-region in parallel for synchronous signal acquisition. In contrast to conventional sequential point-by-point measurement methodologies, electromechanical impedance (EMI) techniques rely on the RMSD metric derived from standalone piezoelectric transducers. Consequently, their diagnostic efficacy is highly susceptible to interference from localized signal perturbations, which manifests as spatially dispersed anomalous high-value indices, thereby impeding precise localization of the underlying damaged domain. The cross-EMI methodology we previously established [16,19] requires supplementary pairwise measurements between adjacent piezoelectric patches, leading to a substantial increase in measurement overhead. Moreover, cross-conductance signatures can only be extracted through dedicated post-processing of the acquired raw datasets. Accordingly, the proposed framework enables significant reduction in overall test duration while preserving robust and reliable damage identification performance.

The remainder of this paper is organized as follows. Section 2 presents the finite element modeling and numerical simulation of damage localization. Section 3 describes the experimental measurements and the corresponding damage localization results. Section 4 introduces the multiplexed parallel acquisition scheme and its experimental verification. Finally, Section 5 summarizes the main conclusions and discusses future work.

2. Damage Localization via FEM Model

2.1. FEM Model and Comparison Study

As illustrated in Figure 1, the steel plate specimen employed in this study has the dimensions of 500 mm in length, 500 mm in width and 3 mm in thickness. The piezoelectric patches were arranged symmetrically on the surface of the steel plate, and the entire monitoring area was divided into 16 damage monitoring sub-regions numbered sequentially from 1 to 16. For the four-edge simply supported steel plate surface-bonded with piezoelectric patches, Liu and Feng [32] derived a closed-form analytical solution for electro-mechanical impedance by jointly considering the in-plane vibration and flexural vibration responses of the structure. The obtained analytical solution has clear physical implications, which can explicitly characterize the influence law of various physical parameters on electro-mechanical impedance signals, and directly reveal the quantitative correspondence between structural physical parameters and output impedance signals. Nevertheless, when internal damage occurs in the thin plate, the local symmetry of the structure is broken, and the symmetry assumption relied on by the original analytical derivation is no longer valid, making it difficult to obtain the corresponding closed-form analytical solution for damaged structures. For this situation, numerical approaches such as the finite element method are required to analyze the electro-mechanical impedance characteristics of damaged structures.

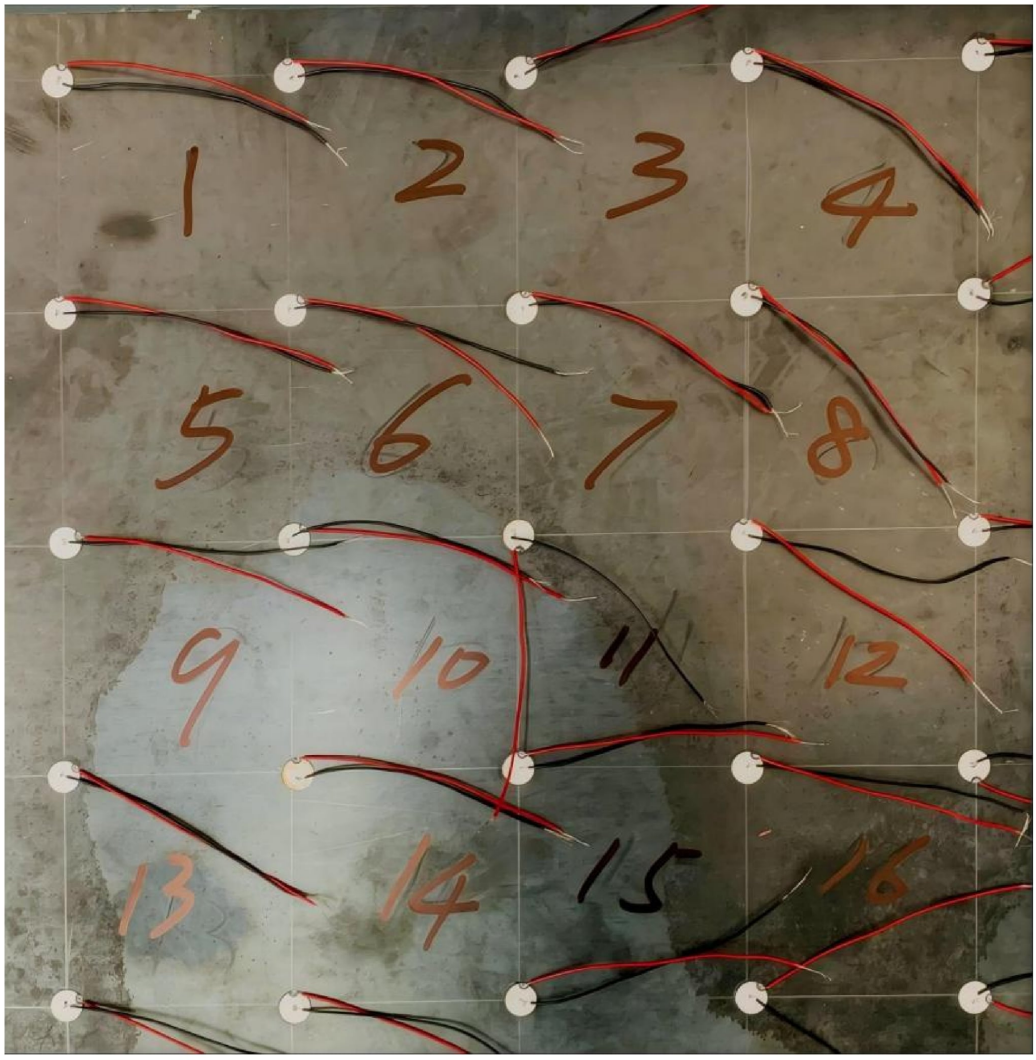


Figure 1. Thin steel plate with surface-bonded piezoelectric patches.

In the finite element simulation, the reasonable selection of element types directly determines the calculation accuracy and computational efficiency, which is of great significance to the whole simulation process. The core idea of finite element analysis is to discretize a continuous structure into a finite number of elements, and approximate the internal displacement and stress field of the structure by using element shape functions. Therefore, the type of element directly determines the mechanical approximation accuracy and solution scale of the discrete model. For thin-plate structural components, the dimension in the thickness direction is far smaller than that in the in-plane direction. Under the action of external loads, the structural response is dominated by in-plane deformation and bending deformation, while the stress variation along the thickness direction is not significant. Therefore, for thin plates with small thickness, discretization using three-dimensional solid elements is not the optimal solution. In comparison, the SHELL63 element in ANSYS is a typical four-node linear shell element constructed based on thin-shell theory. Its mechanical model fully considers the coupling characteristics of in-plane deformation and bending response of thin-plate structures, and is applicable to the mechanical analysis of thin-plate and thin-shell structures whose thickness is much smaller than the planar dimension. The SHELL63 element can effectively reduce the number of elements and the degree of freedom of the model while guaranteeing calculation accuracy, thereby significantly improving calculation efficiency, which is particularly suitable for the dynamic simulation requirements of steel plates bonded with piezoelectric patches.

In the EMI-based finite element analysis, it is not only necessary to consider the inherent mechanical response of the host plate, but also to simultaneously characterize the coupling interaction between the mechanical field and the electric field of the piezoelectric patch, so as to truly capture the response characteristics of the piezoelectric material under external excitation. Conventional finite elements that only contain structural displacement degrees of freedom cannot meet the specific electric field calculation requirements of piezoelectric analysis. Therefore, it is necessary to select piezoelectric elements with multi-physics coupling analysis capability to achieve the simultaneous solution of mechanical field and electric field.

In ANSYS, the available element types that can be used for piezoelectric coupling analysis mainly include PLANE13, SOLID5, SOLID98, SOLID226, and SOLID227. Among these elements, SOLID226 is a three-dimensional 20-node hexahedral solid element. Each node of this element contains both structural displacement degrees of freedom and electric potential degrees of freedom, which can accurately describe the electro-mechanical coupling behavior of piezoelectric materials under the combined action of applied electric field and mechanical load. Benefiting from its excellent numerical stability and high computational accuracy in multi-physics coupling analysis, SOLID226 element has been widely used in research related to the electro-mechanical impedance method [16,19].

The piezoelectric patch utilized in the present investigation is a cylindrical solid with a diameter of 15 mm and a thickness of 0.2 mm. The material parameters of the piezoelectric patch and the steel plate were presented in Tables 1 and 2, respectively. The present analysis assumed ideal perfect bonding at the interface between the piezoelectric patches and the host plate. Constraint-based multi-point constraint (MPC) bonding formulations were implemented to enforce displacement continuity, thereby guaranteeing complete transmission of mechanical deformation between the shell-based steel substrate and the solid piezoelectric patches, with no relative interfacial slip. In this work, the finite element software ANSYS R19.2 was adopted to conduct electro-mechanical impedance (EMI) simulation analysis for the coupled structure composed of the thin plate and the piezoelectric patch.

Table 1. Material properties of piezoelectric patches [19].

Mass Density (kg/m^3)	Dielectric Loss Factor	Flexibility Coefficient S (10^{-12} m^2/N)						Dielectric Constant ε (10^{-8} F/m)		Piezoelectric Strain Constant d (10^{-10} m/V)		
ρ	δ	S_{11}	S_{12}	$S_{22} = S_{33}$	$S_{13} = S_{23}$	$S_{44} = S_{55}$	S_{66}	$\varepsilon_{11}^T = \varepsilon_{22}^T$	ε_{33}^T	$d_{31} = d_{32}$	d_{33}	$d_{15} = d_{24}$
7450	0.0185	15	−4.5	19	−5.7	39	49.4	1.75	2.14	−2.1	5	5.8

Table 2. Material properties of steel plate [19].

Mass Density (kg/m^3)	Elastic Modulus (GPa)	Poisson's Ratio	Damping Ratio
7850	210	0.3	0.01

When an external electric field is applied to piezoelectric materials, dielectric molecules undergo polarization, which further alters the electric field distribution. The permittivity is a key physical parameter characterizing the polarization behaviour of piezoelectric materials. In the ANSYS finite element platform, the permittivity matrix of polarized piezoelectric materials is symmetric and contains only three independent components. Therefore, the permittivity matrix can be expressed as follows:

$$[\varepsilon] = \begin{pmatrix} \varepsilon_{11} & 0 & 0 \\ 0 & \varepsilon_{22} & 0 \\ 0 & 0 & \varepsilon_{33} \end{pmatrix}, \tag{1}$$

The piezoelectric matrix describes the coupling relationship between the electrical and mechanical behaviors of piezoelectric materials, and it mainly exists in two forms: the piezoelectric strain matrix and the piezoelectric stress matrix. The piezoelectric stress matrix **e** is associated with the compliance matrix **s**, so these two matrices can be converted into each other, and their relationship is expressed as:

$$\mathbf{e} = \mathbf{s}^{-1}\mathbf{d}, \tag{2}$$

First, the material coefficients and element attributes were assigned to each structural component. Subsequently, an alternating voltage of 1 V was applied to the upper and lower surfaces of the PZT patches. The charge quantity Q was extracted via the TimeHist Postpro module in the ANSYS GUI. The electro-mechanical admittance Y is then calculated using the formula below.

$$Y = \frac{I}{V} = \frac{\partial Q/\partial t}{V} = i\omega\frac{Q}{V}, \tag{3}$$

The conductance spectrum acquired via finite element method (FEM) simulation was compared with that obtained from the theoretical analytical solution [27]. As illustrated in Figure 2, the two conductance spectra extracted through different methods demonstrated satisfactory overall consistency. In particular, the peak positions corresponding to the resonance frequencies were in good agreement, which validated the accuracy of the proposed finite element model. On this basis, subsequent sections of this paper will carry out damage identification research based on this established model.

Mesh sensitivity and convergence analyses for the finite element model were also carried out using three element sizes: 2 mm, 2.5 mm and 5 mm. As illustrated in Figure 3, the influence of element size on the numerical accuracy is evaluated by comparing the harmonic response results from these three discretization cases. Comparative analysis demonstrates that finite element model predictions obtained using element sizes of 2 mm and 2.5 mm exhibit near-identical agreement. Balancing computational accuracy and numerical efficiency, an element size of 2.5 mm is adopted for all subsequent simulations.

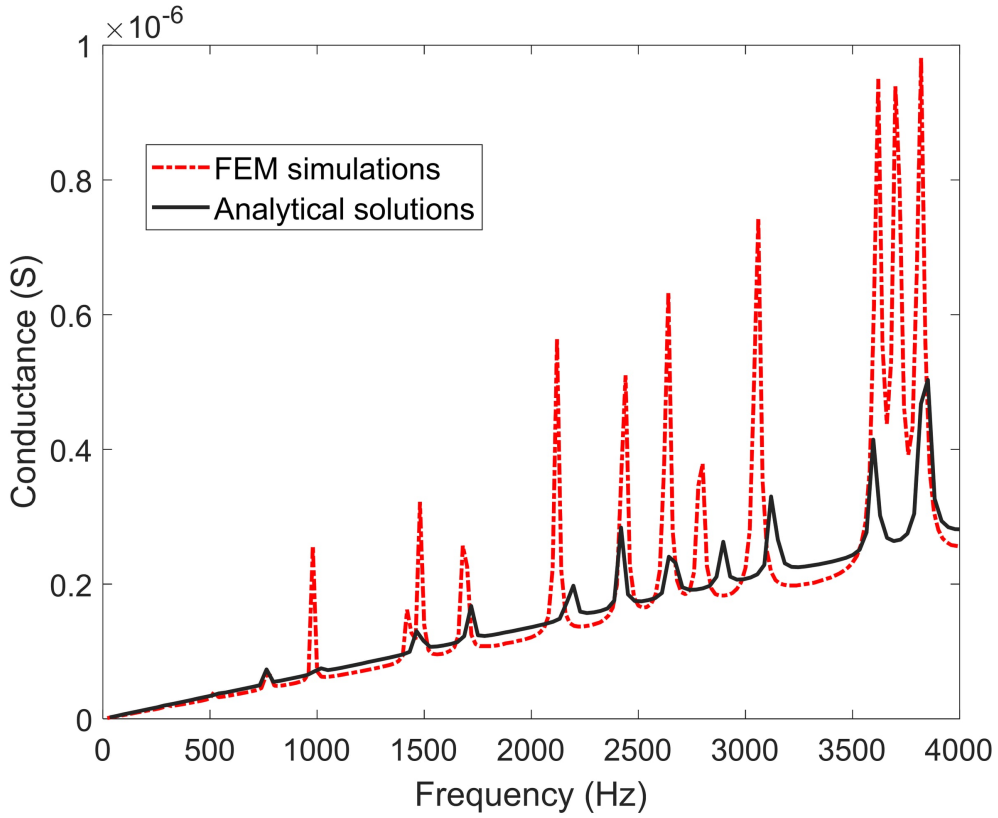


Figure 2. Comparison between FEM results and analytical solutions.

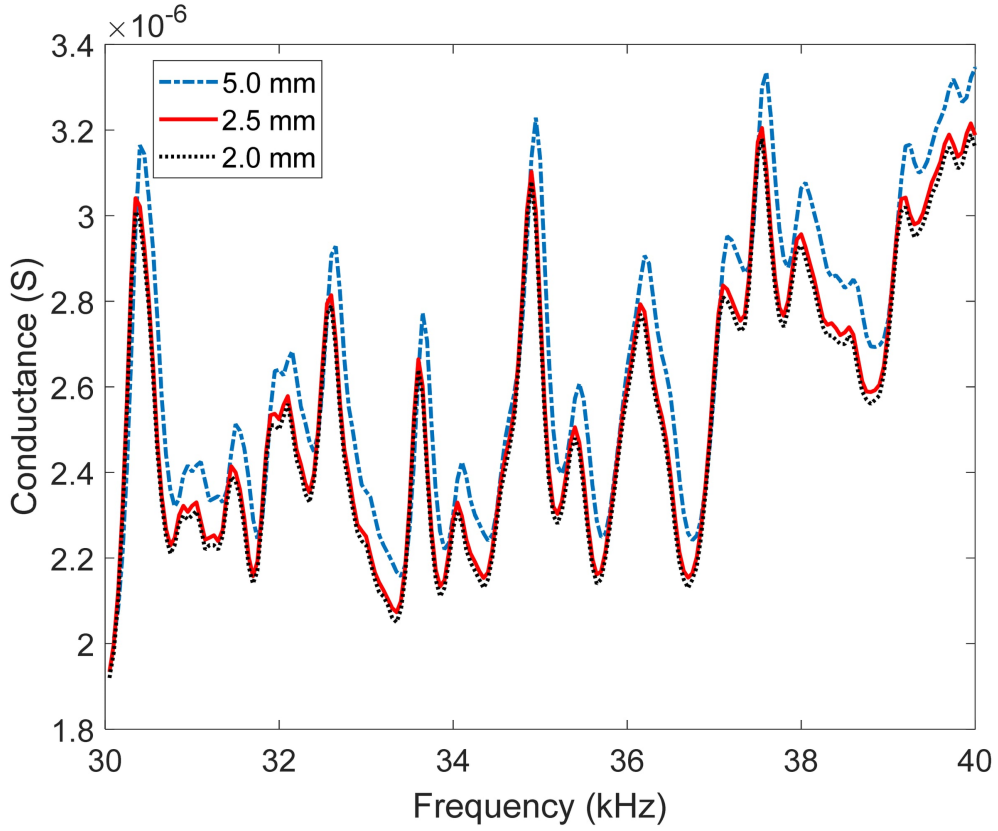


Figure 3. Mesh convergence analysis with different element sizes.

2.2. EMI Signals Based on Proposed Model

Based on the aforementioned verified finite element model, the present paper performed a numerical simulation investigation on damage location identification of steel thin plates. As presented in Figure 4, 25 piezoelectric patches were symmetrically deployed on the surface of the target thin plate, and such a layout divides the entire steel thin plate into 16 independent regions. To simulate structural damage, a circular hole with a diameter of 15 mm was prefabricated at the geometric center of Region 7 to serve as the artificial damage [33–35], and the piezoelectric patches surrounding the damage location were numbered 8, 9, 13, and 14. In the process of numerical simulation, a unit alternating voltage was applied sequentially to each piezoelectric patch [23], and harmonic response analysis was implemented for both the undamaged and damaged states of the thin plate. Given that high-frequency structural responses are more sensitive to local damage, the frequency range of 30–40 kHz was selected for the present analysis. Finally, the conductance spectra corresponding to each piezoelectric patch under the undamaged and damaged states were extracted via harmonic response analysis.

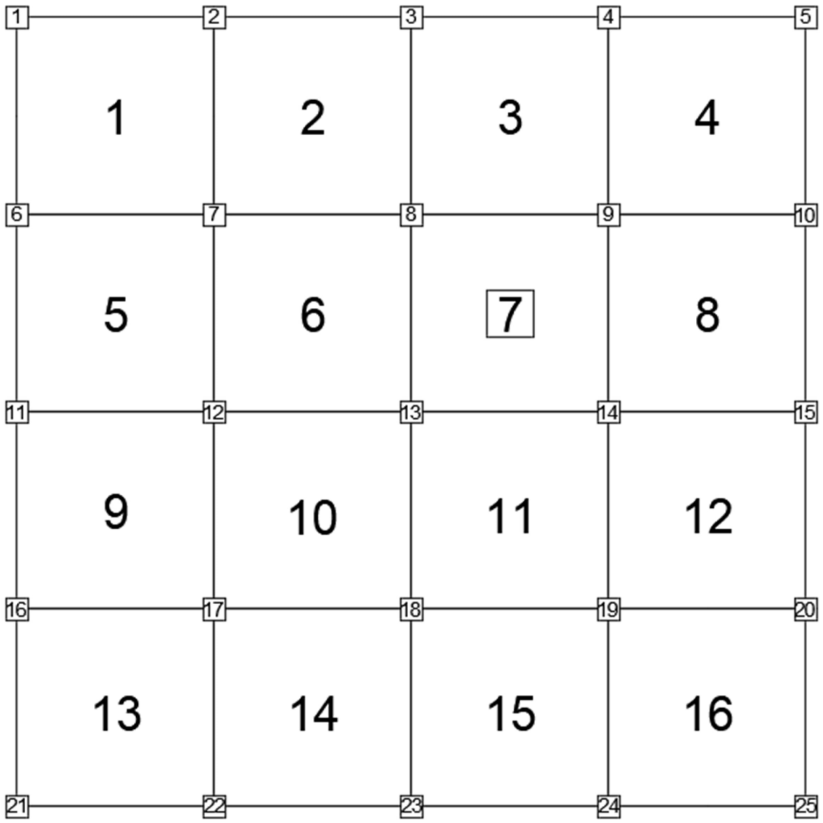
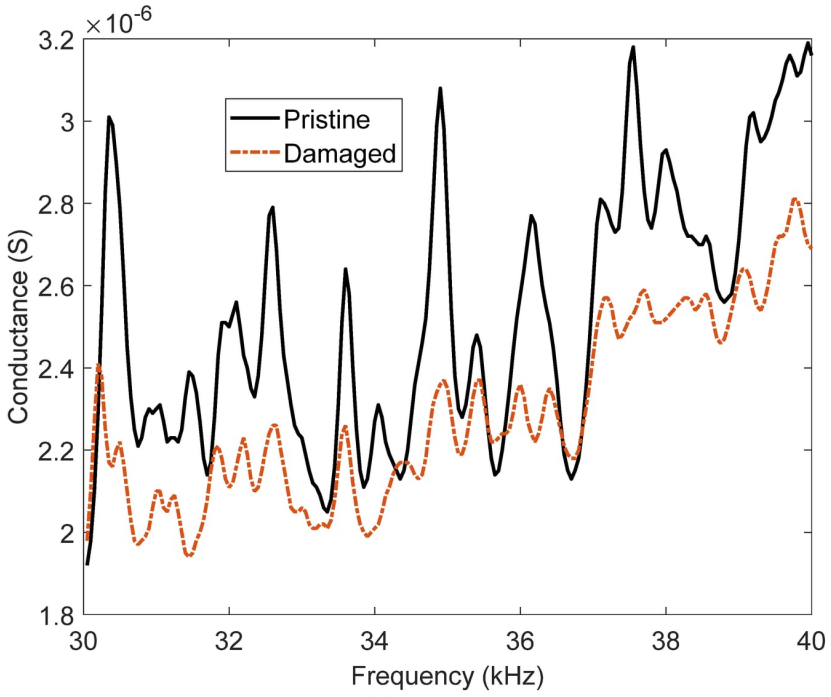


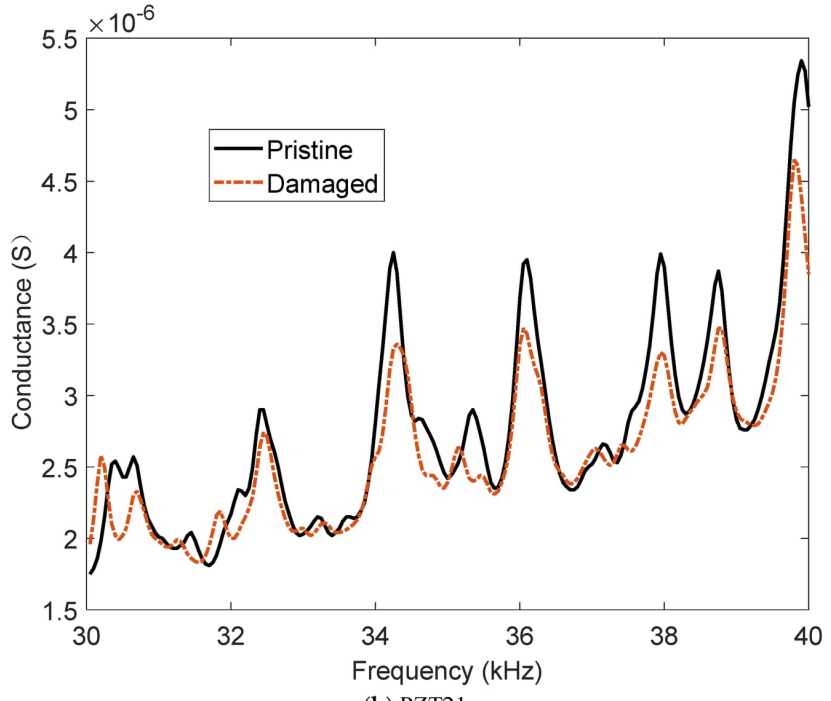
Figure 4. Schematic diagram of rectangular specimen.

For the sake of brevity, only piezoelectric Patch 9 adjacent to the damaged area and Patch 21 distant from the damage were selected as typical samples for demonstration. As shown in Figure 5, for Patch 9 located in proximity to the damaged region, the conductance spectra acquired under the damaged and undamaged conditions exhibited an obvious peak deviation. In comparison, for Patch 21 located far from the damaged region, the difference between the conductance spectra under the two working states was relatively insignificant. The numerical results further validated the correlation between the variation amplitude of piezoelectric conductance signals and the distance to the damage location: the farther a piezoelectric patch is from the damage location, the smaller the variation amplitude of its conductance signal. Relying on this characteristic, preliminary damage location judgment

can be implemented. However, direct visual inspection of conductance spectra cannot explicitly and quantitatively reflect the signal discrepancies among different piezoelectric patches. Hence, it is essential to introduce statistical damage indices to perform damage location identification analysis for the thin plate. Statistical damage indices can quantitatively characterize the magnitude of discrepancy between two datasets, and have better intuitiveness, higher objectivity and greater identification efficiency than direct observation of conductance spectra.



(**a**) PZT 9



(**b**) PZT21

Figure 5. Simulated EM conductance for pristine and damaged plates based on FEM.

2.3. Methodology

Structural damage assessment methods based on statistical damage indices have currently become a technical approach that is preferentially selected by many researchers [36–39], owing to their outstanding advantages, including simple operation, intuitive output results and high identification accuracy and efficiency. By comparing conductance signatures collected from each piezoelectric sensing point against the corresponding healthy baseline, statistical damage indices can effectively capture changes in the internal mechanical state of the structure. This provides a reliable technical basis for structural damage detection and assessment in engineering applications. Currently, in the research fields of EMI-based damage identification technology, the Root Mean Square Deviation (RMSD) damage index has been widely applied to quantitatively evaluate the difference degree between the actually measured data and the baseline reference data, so as to further assist in judging the occurrence of structural damage and identifying the specific location of damage. The specific expression of the RMSD damage index is given as follows [26–31,36]:

$$\mathrm{RMSD} = \sqrt{\frac{\sum_{i=1}^{i=N}(y_i - x_i)^2}{\sum_{i=1}^{i=N} x_i^2}} \tag{4}$$

where x_i and y_i denote the conductance values acquired at the i-th measurement point in the undamaged baseline state and damaged working condition, respectively. Since EMI signals exhibit higher sensitivity to local damage occurring in their adjacent regions, the location of structural damage can be readily determined by comparing the RMSD values corresponding to different measurement points [19]. According to the electromechanical coupling principle, changes in structural mechanical impedance will be reflected in the measured electrical admittance signature of surface-bonded piezoelectric patches. The deviation between damaged-state and healthy-state admittance is quantified by the RMSD damage index. Accordingly, piezoelectric patches near the defect yield higher RMSD values.

Existing studies have shown that directly applying statistical damage indices to process raw conductance data may introduce calculation deviations, which are induced by the characteristic discrepancies among individual piezoelectric patches and environmental variations such as temperature fluctuations across different tests [4,19]. To resolve this issue, the Z-score standardization method was adopted in this study. The conductance data was processed via Z-score standardization first, and the statistical damage index was then calculated based on the standardized dataset. The expression of Z-score standardization is given as follows [4,19]:

$$z_i = \frac{x_i - \overline{x}}{\sigma} \tag{5}$$

where x_i and $\overline{x}$ denote the raw conductance data and the mean value of the conductance dataset, σ is the standard deviation of the conductance dataset, and z_i is the conductance data after Z-score standardization, respectively.

2.4. Results and Discussion

The simulated data acquired from all piezoelectric patches were processed individually, and the conductance signal amplitudes within the frequency range of 30 kHz to 40 kHz were extracted. The extracted conductance values were first subjected to Z-score standardization processing, after which the corresponding RMSD statistical index was calculated. The magnitude of the RMSD value can characterize the spatial correlation between the piezoelectric patch and the damage location. A higher RMSD value indicates that the corresponding piezoelectric patch is located closer to the damage site. As illustrated in Figure 6, the maximum RMSD values were acquired at piezoelectric patches No. 13 and No. 9, while the RMSD values of piezoelectric patches No. 8 and No. 14 also stayed at

relatively high magnitudes. Based on the above results, the damage can be preliminarily determined to be approximately located in Region 7. Nevertheless, the RMSD values of piezoelectric patches No. 10 and No. 17 also remained at relatively high magnitudes, and relying solely on the RMSD index extracted from a single piezoelectric patch still cannot accurately pinpoint the specific scope of the damage. To address the problem of insufficient positioning accuracy of single piezoelectric patch-based damage indices, this paper further proposed a regional statistical method. The arithmetic average was calculated for the RMSD damage indices of the four piezoelectric patches surrounding each region, and this average value was employed as the comprehensive damage identification damage index of the corresponding region, so as to realize intuitive comparison of damage response intensities among different regions. Through analyzing the regional average RMSD values output by the proposed finite element model, it can be clearly observed from Figure 7 that the maximum RMSD value occurs in Region 7, where the pre-set damage is located. The conventional single-patch electromechanical impedance (EMI) approach relies on the root-mean-square deviation (RMSD) parameter extracted from each standalone piezoelectric transducer. Its diagnostic performance is readily compromised by localized signal fluctuations, manifesting as spatially dispersed high-value indicators that hinder the precise localization of actual damaged regions. In contrast, the proposed regional averaging methodology mitigates random perturbations by averaging the RMSD outputs derived from four adjacent sensors, and exclusively requires drive-point measurements. This configuration effectively enhances the distinguishability of damaged regions. It should be noted that the numerical labels in the bar chart respectively correspond to the numbering of piezoelectric patches and the sub-regions divided on the steel thin plate, which were depicted in Figures 5 and 6 in sequence.

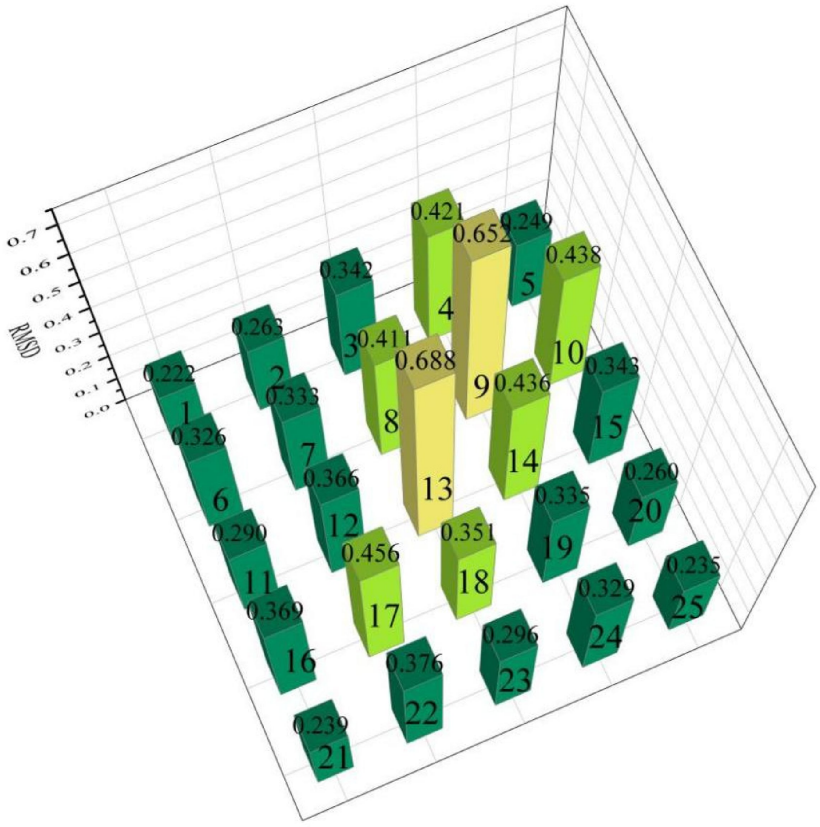


Figure 6. FEM-simulated RMSD values from each piezoelectric patch *. (* The numbers on the bar chart denote the piezoelectric patch numbers.)

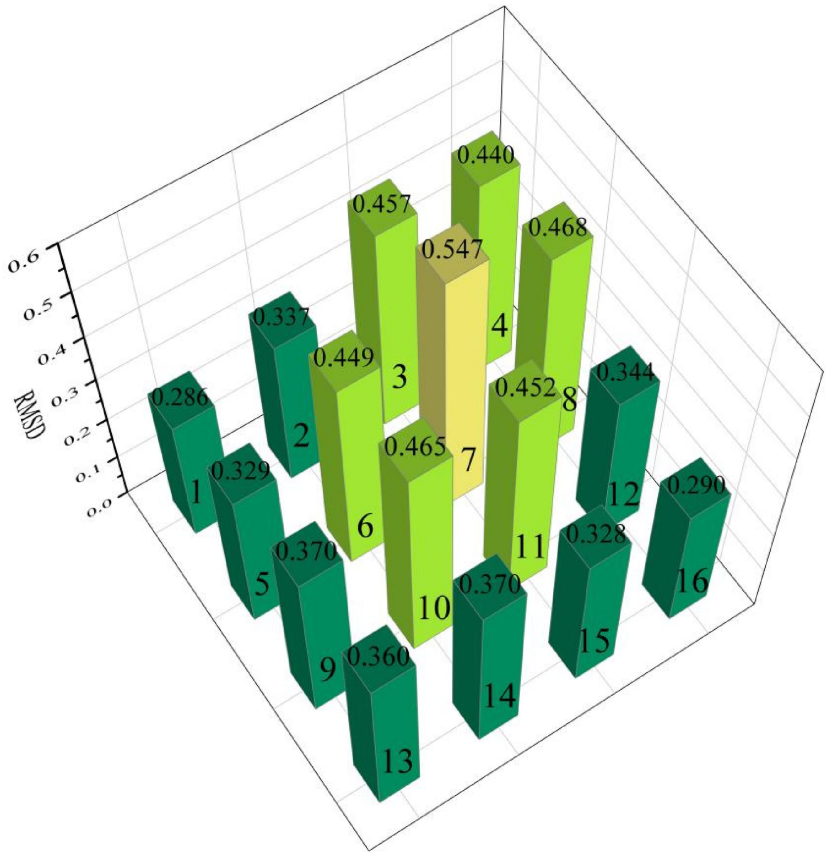


Figure 7. FEM-simulated RMSD values obtained from the average of four piezoelectric patches *. (* The numbers on the bar chart denote the numbers of sub-regions divided on the thin plate.)

3. Damage Localization via Experimental Measurements

3.1. Experimental Set-Up

The piezoelectric patches used in this experiment were fabricated by Suzhou Pante Electronic Ceramics Technologies Co., Ltd., Suzhou, China, with the product model specified as HNYA16-0.41-1. Each piezoelectric patch, which has a diameter of 15 mm and a thickness of 0.2 mm, was symmetrically attached to the steel specimen using 502 super glue (Ningbo Deli Group Co., Ltd., China). Note that before testing, the adhesively bonded transducer must be cured for 24 h to avoid data drift. The piezoelectric patch was fixed on the surface of the tested steel plate by adhesive bonding, its two electrode layers were arranged coplanarly, and they were respectively led out via wires of different colors for polarity differentiation. The configuration of the experimental specimen was consistent with that adopted in the numerical simulation, and a steel plate with a plane dimension of 500 mm × 500 mm and a thickness of 3 mm was selected as the test specimen.

Similar to the finite element numerical simulation, the plate was divided into 4 rows and 4 columns, resulting in a total of 16 regions, and 5 rows and 5 columns of measurement points (25 in total) were arranged correspondingly. One piezoelectric patch was bonded at each measurement point, thereby constructing a piezoelectric sensor array covering the entire surface of the steel plate. The specific region-numbering scheme and the measurement-point layout were presented in Figures 3 and 7, respectively. In the present experiment, structural damage was simulated by drilling a circular hole with a diameter of 15 mm at a pre-designed position on the steel plate [33–35], and the damage was also arranged in Region 7. This arrangement ensures that the experimental working conditions are completely consistent with those adopted in the numerical simulation. All piezoelectric patches were connected

sequentially to the impedance analyzer through wires to apply voltage excitation and collect the impedance response signals. The experimental setup employed a WK6500B impedance analyzer manufactured by Wayne Kerr Electronics, Shenzhen, China, and the complete connection configuration of the experimental instrument was presented in Figure 8. Given the heightened sensitivity of high-frequency signals to structural damage, the test frequency interval was set to 30–40 kHz. To fully capture the variation trends of drive-point admittance, 800 sampling points were evenly allocated across this bandwidth. Additionally, two separate repeated measurement runs were conducted under temperature-controlled laboratory conditions maintained by air conditioning.

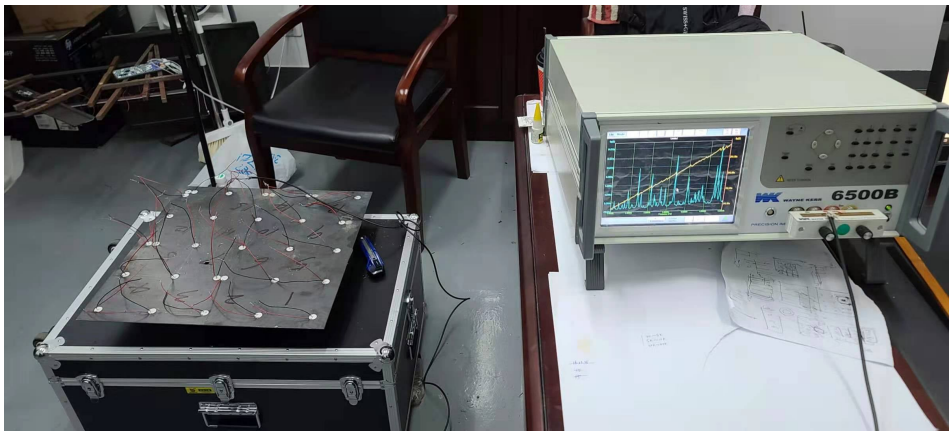


Figure 8. Experimental setup.

3.2. Measured EMI Signals

For brevity, only PZT 9, which is located adjacent to the damaged region, and PZT 21, positioned far from the damage location, were selected as representative cases for the subsequent analysis. As shown in Figure 9, the conductance curves of PZT 9 located proximal to the damage region exhibited significant discrepancy between the intact and damaged structural states. This confirmed that the piezoelectric patch at this position has high sensitivity to the variation in local structural impedance induced by structural damage. As depicted in Figure 10, for PZT 21 located in the undamaged region, the difference between its conductance curves under the two structural states was relatively minor, which indicated that piezoelectric patches distant from the damage location have low response sensitivity to structural damage. The experimental results further verified that the piezoelectric conductance response has a distance-dependent characteristic, which varies with the spatial distance between the piezoelectric patch and the damage.

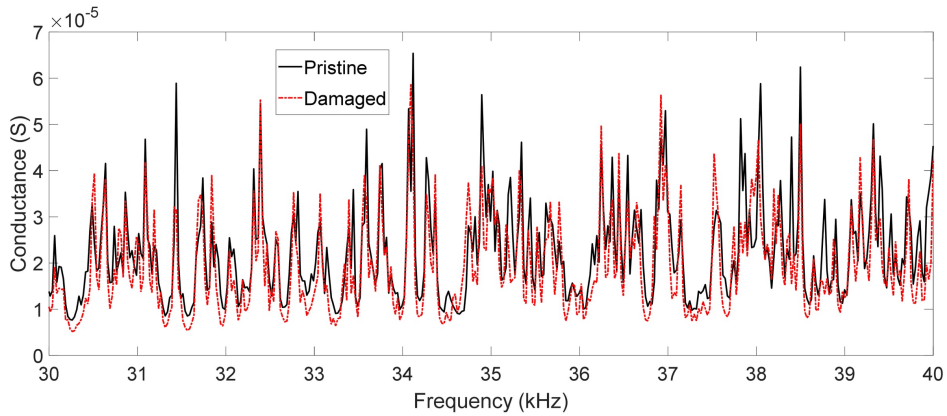


Figure 9. Measured EM conductance for PZT 9 under pristine and damaged states.

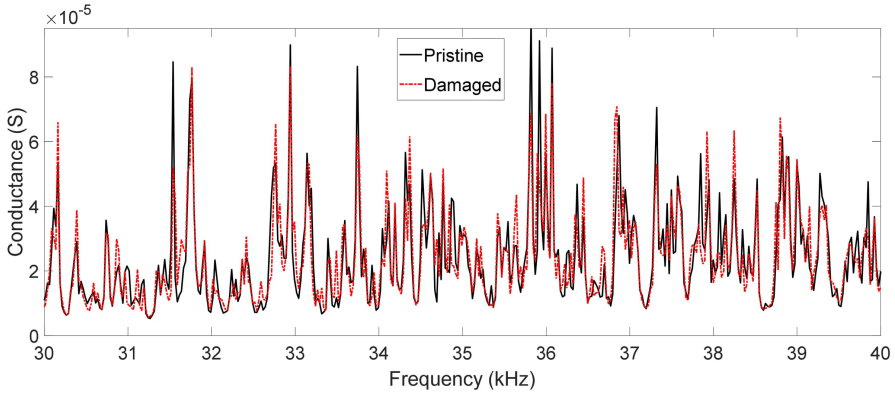


Figure 10. Measured EM conductance for PZT 21 under pristine and damaged states.

Compared with the simulated EMI curves in Figure 5, the experimental results exhibit a richer set of resonant peaks. This phenomenon has also been documented in previous cross-EMI tests on bolted joints and beam structures [16,19]. Four primary factors account for this discrepancy. First, high-frequency excitation excites dense structural modes and local secondary vibration modes, such as thickness-wise vibration. The present finite-element model is established based on two-dimensional shell theory, which only captures global flexural and axial vibrations and cannot replicate these local secondary modes. Second, homogeneous material properties (mass density, damping ratio, elastic modulus) are assigned in the numerical model, whereas real specimens possess spatially non-uniform material characteristics; such inhomogeneity is greatly amplified under high-frequency excitation [16,19]. Third, a constant, frequency-independent damping value is used for the steel plate, PZT patches and bonding layer in simulation. In practice, material and interfacial damping are frequency-dependent. Greater damping loss at high frequencies reshapes the measured spectra, an effect that cannot be fully represented by the simplified numerical model. Finally, ideal perfect bonding is assumed in the simulation. In physical specimens, subtle spatial variations in adhesive thickness and local interfacial defects further distort the measured EMA spectra. Accordingly, the predictive performance of the model degrades when abundant local vibration responses beyond the assumptions of thin-plate theory are triggered. Within the 30–40 kHz frequency band selected for damage localization, the proposed model is capable of reproducing the trend of EMA spectral variations induced by damage, although precise quantitative agreement on all resonant peaks between simulation and experiment is not expected.

3.3. Results and Discussion

Subsequently, Z-score standardization was performed on the conductance data measured from all piezoelectric patches, and the corresponding RMSD statistical indices were calculated thereafter. Based on the comparison results of RMSD damage indices for individual piezoelectric patches presented in Figure 11, the peaks of the RMSD curve correspond to the No. 8 piezoelectric patch and No. 15 piezoelectric patch, respectively. This result only allows a preliminary inference that potential damage is likely to be distributed in Region 7 or Region 8, and a unique and deterministic determination of the actual damage region cannot be obtained. Based on the conclusions obtained from previous finite element analyses, averaging statistical damage indices can effectively improve the identification accuracy of damage localization. Accordingly, this investigation further carried out averaging processing on the RMSD damage indices of each piezoelectric patch acquired from the thin-plate experiment. As shown in Figure 12, the processing results demonstrated that the maximum RMSD value was definitively concentrated in Region 7, with the damage localization result

being clearly distinguishable. These results further validate that the regional averaging method outperforms the traditional drive-point measurement approach.

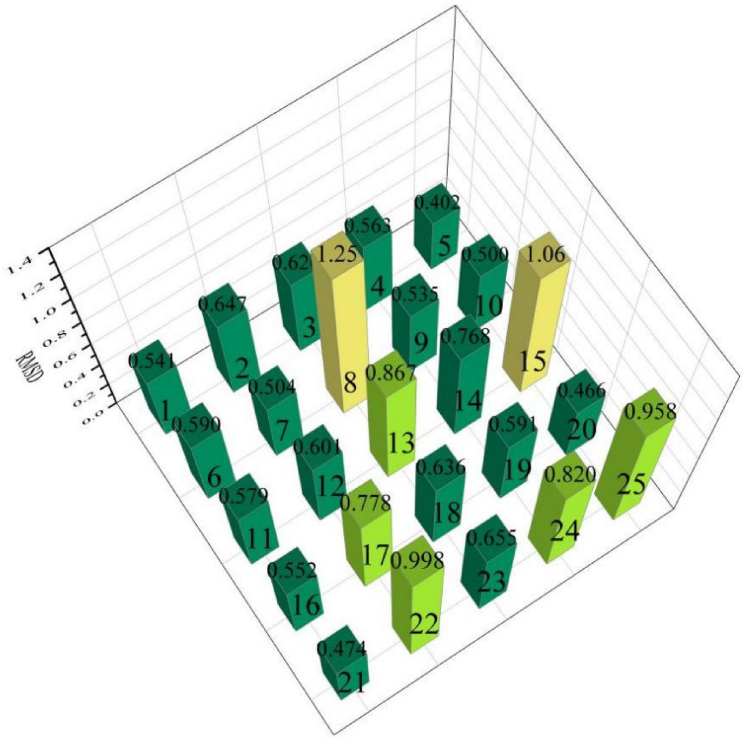


Figure 11. RMSD values calculated from the measurements collected by each piezoelectric patch *. (* The numbers on the bar chart denote the piezoelectric patch numbers.)

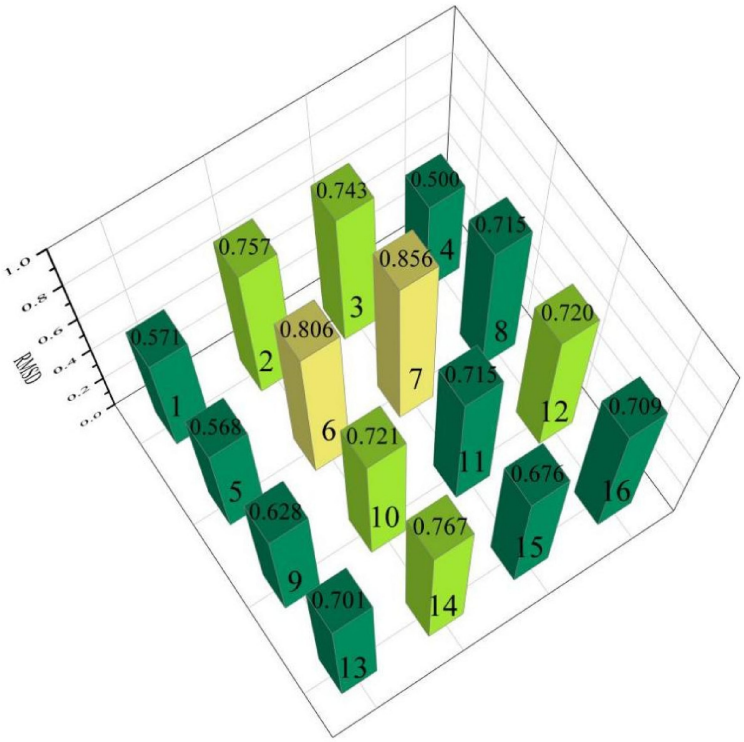


Figure 12. RMSD values obtained via averaging the measurements of four piezoelectric patches *. (* The numbers on the bar chart denote the numbers of sub-regions divided on the thin plate.)

4. Damage Localization via Multiplexed Parallel Acquisition

4.1. Principle of Multiplexed Parallel Acquisition

In sequential damage identification experiments conducted on plate structures, individual testing of every piezoelectric patch at all measurement points not only leads to an excessively large testing workload, but also introduces significant time cost, thereby substantially constraining the applicability of conventional sequential measurement frameworks in practical engineering scenarios. To enhance the efficiency of damage detection for plate structures, this paper proposed an improved testing scheme that allows for synchronous acquisition and analysis of output signals from multiple piezoelectric patches, thus effectively compressing the overall measurement duration while ensuring the completeness of the acquired information. As shown in Figure 13, during the testing procedure, the four piezoelectric patches contained within each regional grid were connected in parallel to realize synchronous signal acquisition across multiple measurement points, which reduced the number of independent measurement steps required for covering the entire sensing network. Furthermore, multiplexed parallel acquisition electrically connects multiple piezoelectric patches in parallel to directly measure the combined cross electro-mechanical admittance of the sensor cluster, which is fundamentally different from the conventional drive-point admittance measured individually from each single piezoelectric transducer. Instead of separately acquiring admittance signals from every patch, this scheme obtains the integrated cross-EMA response of a regional sensor group in one measurement. Compared with traditional point-drive admittance, the cross admittance carries coupled vibration information originating from the whole sensing region [16,19]. It retains damage-sensitive features for regional damage identification while reducing the total number of measurement channels and shortening the testing duration. This characteristic makes it efficient for fast screening and localizing damage within the plate, without sacrificing the capability to capture the relative spectral changes used for RMSD-based damage evaluation. Theoretically, the equivalent admittance formula for four parallel-connected piezoelectric patches is expressed as

$$Y = \sum_{i=1}^{4} \sum_{j=1}^{4} Y_{ij} \tag{6}$$

where $Y_{ij}(i = j)$ denotes drive-point conductance. When $i \neq j$, we can obtain cross conductance.

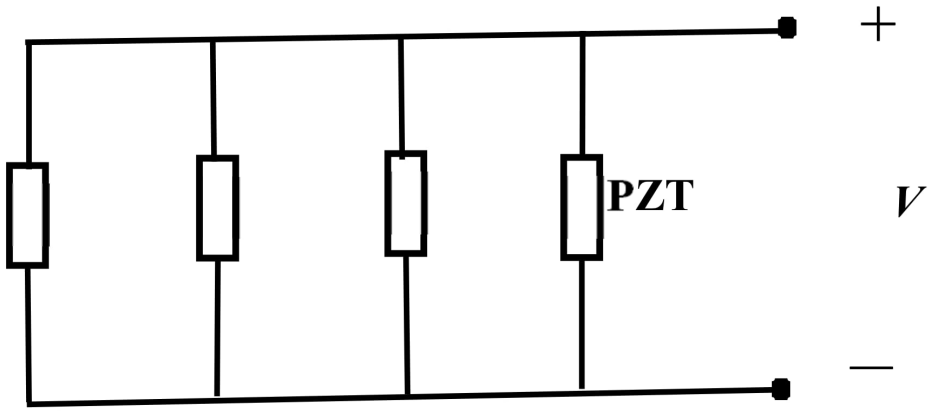


Figure 13. Schematic diagram of multiplexed parallel acquisition.

4.2. Results and Discussion

Taking the damaged plate specimen as the research example, the experimentally measured conductance curves of the four piezoelectric patches (No. 8, 9, 13, 14) surrounding

the damage-containing region (i.e., Region 7) under the damaged condition, along with the corresponding conductance curves acquired under the intact condition, were plotted in Figure 14. The experimental results showed that the conductance curves acquired under the damaged condition exhibited a significant offset relative to those obtained under the intact condition, indicating that the introduction of structural damage produces a discernible change in the local EMI response characteristics. To conduct a further controlled comparative analysis, four piezoelectric patches were randomly selected from the undamaged region (i.e., Region 13). Following the identical processing procedure, the conductance curves of the selected piezoelectric patches under both damaged and intact conditions were plotted in Figure 15.

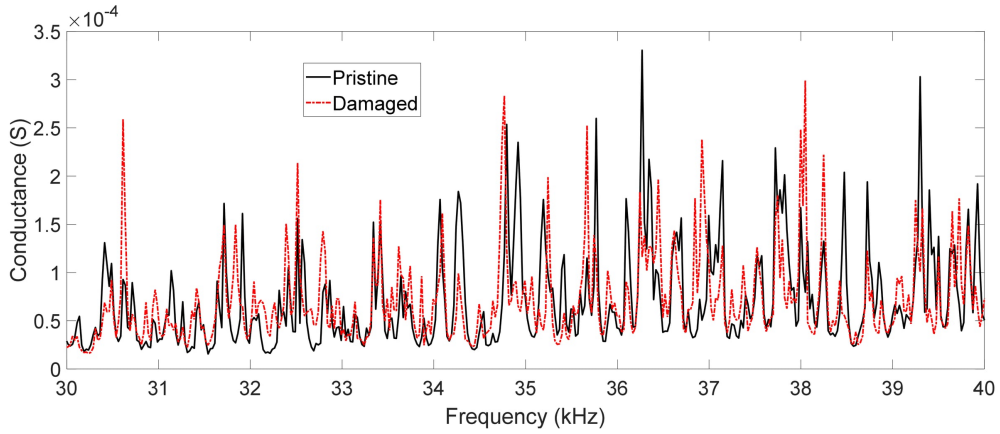


Figure 14. Measured EM conductance via multiplexed parallel acquisition (Region 7).

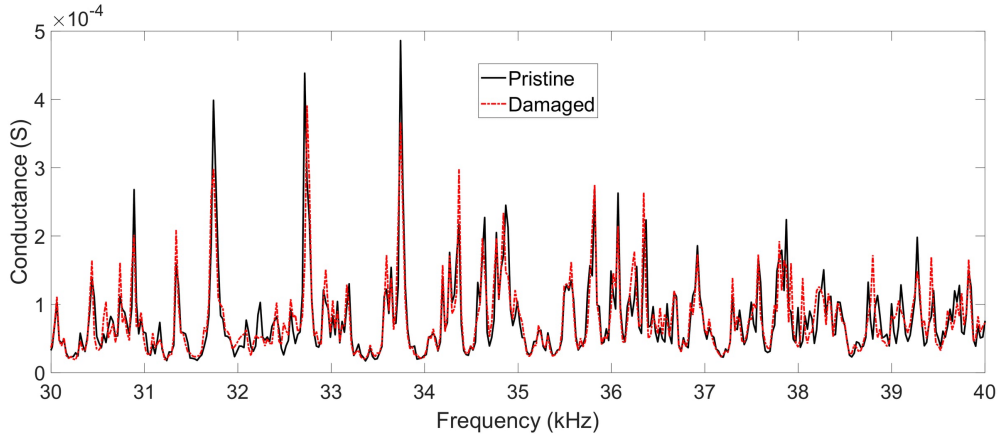


Figure 15. Measured EM conductance via multiplexed parallel acquisition (Region 13).

A comparative analysis of the results presented in Figures 14 and 15 demonstrated that, in comparison with the conductance curves obtained from the undamaged region, the conductance curves acquired from the damaged region exhibited more pronounced peak variations and greater deviations between the damaged and intact structural states. This experimental observation confirmed that in structural damage detection, the closer a measurement point is to the damage site, the more significant the variation amplitude of its conductance curve in the damaged state relative to the intact state will be, which verified the spatial sensitivity of the EMI response to local structural changes.

In the present study, conductance data within the 30–40 kHz frequency band were also selected for further analysis, because this frequency range has been demonstrated to contain sufficient structural dynamic information for damage-sensitive feature extraction. After

standardization processing of the acquired conductance data, the bar chart corresponding to the statistical damage index of each sub-region was plotted, with the results shown in Figure 16. As can be seen from Figure 14, the maximum RMSD value was located in Region 7, based on which the damage location can be accurately identified.

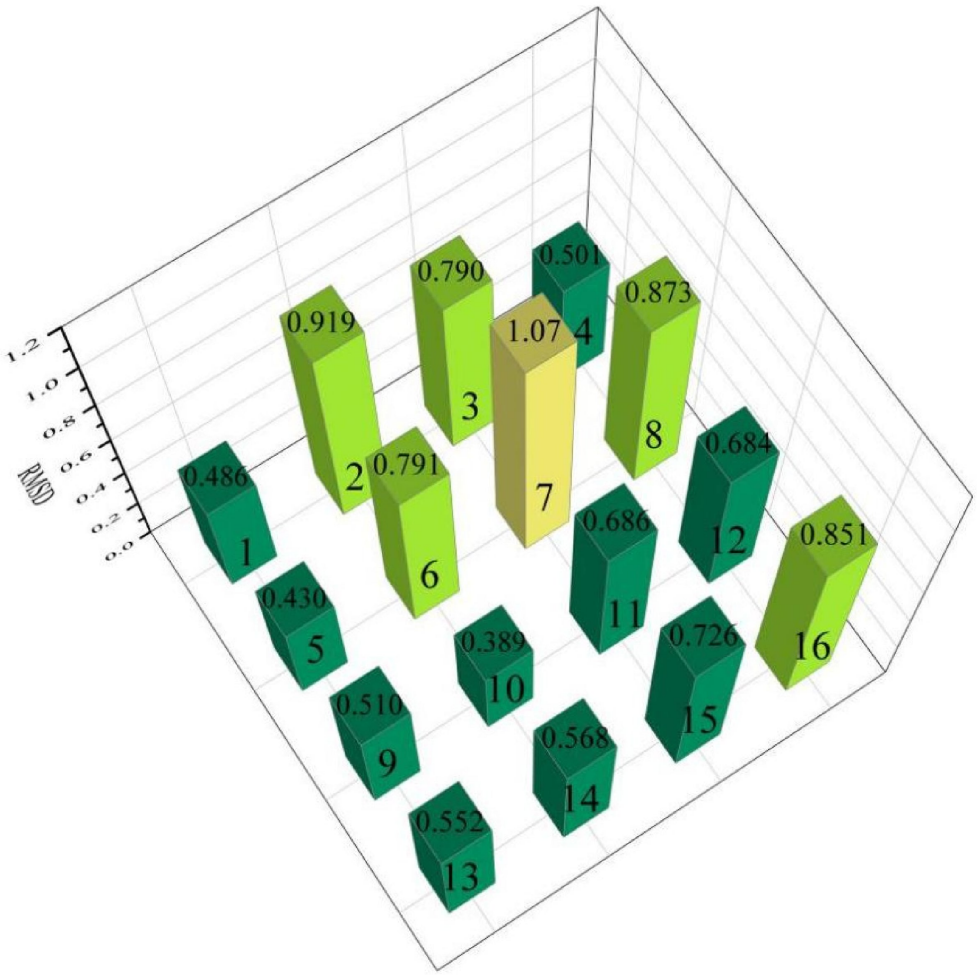


Figure 16. RMSD values obtained via multiplexed parallel acquisition *. (* The numbers on the bar chart denote the numbers of sub-regions divided on the thin plate.)

5. Conclusions

This study investigated damage localization in thin steel plates using EMI signals acquired from a distributed piezoelectric sensor array. Both finite-element numerical simulations and laboratory experimental tests were carried out, and an improved damage index processing strategy together with a multiplexed parallel acquisition scheme was proposed to achieve efficient damage identification for plate-type structures.

The FEM simulations exhibited good agreement with the analytical solutions, confirming the computational accuracy of the established model. Based on the validated model, the numerical results indicated that the piezoelectric patches adjacent to the damaged region yielded significantly higher RMSD values, while those far from the damage presented relatively lower values, confirming that the sensitivity of EMI-based detection depends on the distance between the sensing element and the damage location. To further improve localization accuracy, a regional statistical method was proposed by averaging the RMSD values of the four piezoelectric patches surrounding each sub-region, and the damaged region was accurately identified as the one with the maximum regional average RMSD.

Experimental measurements on a steel plate specimen with the distributed sensor array further verified the effectiveness of the proposed method.

To address the heavy workload and prolonged time consumption associated with sequential point-by-point measurement, a multiplexed parallel acquisition scheme was further developed by connecting the four piezoelectric patches within each monitoring sub-region in parallel for synchronous signal acquisition. Experimental results demonstrated that the signals collected via multiplexed parallel acquisition could still capture significant spectral deviations induced by local damage and accurately locate the actual region containing damage. The proposed approach effectively shortens the overall testing duration while maintaining reliable damage identification performance, offering a promising technical solution for efficient structural health monitoring of plate structures.

Nevertheless, the present study has several inherent limitations. First, all validations were performed on only one steel plate specimen with a single type of circular-hole damage, and the layout of the distributed piezoelectric array was not optimized. Second, the influences of external service loads, varying boundary conditions, degradation and thickness inhomogeneity of the adhesive layer, and temperature fluctuations were not considered in the numerical and experimental investigations. In addition, the method was validated only within the selected frequency range of 30–40 kHz, and its adaptability to other frequency bands remains to be explored. It should also be clarified that the proposed method can only realize regional damage identification rather than pinpointing the exact damage coordinates. Therefore, direct extension to large-scale practical engineering structures still requires further systematic verification under complex service environments.

Author Contributions: Conceptualization, W.Y. and L.Y.; Methodology, W.Y.; software, L.Y.; validation, W.Y.; investigation, L.Y.; writing—original draft, L.Y.; writing—review and editing, W.Y.; supervision, W.Y.; funding acquisition, W.Y. All authors have read and agreed to the published version of the manuscript.

Funding: Applied Research Project of Public Welfare Technology in Zhejiang Province (grant number LGF21E080004) and National Natural Science Foundation of China (grant number 12572173).

Data Availability Statement: The data presented in this study are available from the corresponding author upon reasonable request.

Conflicts of Interest: The authors declare no conflicts of interest.

References

1. Mohammadi, M.; Rashidi, M.; Azandariani, M.G.; Mousavi, V.; Yu, Y.; Samali, B. Modern Damage Measurement of Structural Elements: Experiment, Terrestrial Laser Scanning, and Numerical Studies. *Structures* **2023**, *58*, 105574. [CrossRef]
2. Yang, Z.; Ai, D.M.; Zhu, H.P. Heterogeneous Mesoscale Concrete Model Bonded with PZT Sensor for Electromechanical Admittance-Based Structural Damage Identification. *Smart Mater. Struct.* **2025**, *34*, 035039. [CrossRef]
3. Naoum, M.C.; Chalioris, C.E.; Karayannis, C.G.; Karabinis, A.I.; Elenas, A. Electro-Mechanical Impedance-Based Structural Health Monitoring of Fiber-Reinforced Concrete Specimens under Four-Point Repeated Loading. *CivilEng* **2023**, *4*, 856–880. [CrossRef]
4. Sapidis, G.M.; Kansizoglou, I.; Naoum, M.C.; Papadopoulos, N.A.; Chalioris, C.E. A Deep Learning Approach for Autonomous Compression Damage Identification in Fiber-Reinforced Concrete Using Piezoelectric Lead Zirconate Titanate Transducers. *Sensors* **2024**, *24*, 386. [CrossRef] [PubMed]
5. Lee, J.C. Evaluation of Setting Times of Concrete Using Electro-Mechanical Impedance Sensing Technique. *Materials* **2023**, *16*, 5618. [CrossRef] [PubMed]
6. Winklberger, M.; Kralovec, C.; Humer, C.; Heftberger, P.; Schagerl, M. Crack Identification in Necked Double Shear Lugs by Means of the Electro-Mechanical Impedance Method. *Sensors* **2021**, *21*, 44. [CrossRef] [PubMed]
7. Baral, S.; Negi, P.; Adhikari, S.; Bhalla, S. Temperature Compensation for Reusable Piezo Configuration for Condition Monitoring of Metallic Structures: EMI Approach. *Sensors* **2023**, *23*, 1587. [CrossRef] [PubMed]
8. Sahm, D.; Pak, D. Influence of Temperature and Preload Force on Capacitance and Electromechanical Impedance of Lead Zirconate Titanate Piezoelectric Wafer Active Sensors for Structural Health Monitoring of Bolts. *Appl. Phys. A* **2024**, *130*, 156. [CrossRef]

9. Parida, L.; Moharana, S.; Vicente, R.; Ascensao, G. A Proof of Concept Study on Reliability Assessment of Different Metal Foil Length Based Piezoelectric Sensor for Electromechanical Impedance Techniques. *Sci. Rep.* **2024**, *14*, 699. [CrossRef] [PubMed]
10. Bansal, T.; Talakokula, V.; Sathujoda, P. Machine Learning-Based Monitoring and Predicting the Compressive Strength of Different Blended Cementitious Systems Using Embedded Piezo-Sensor Data. *Measurement* **2022**, *205*, 112204. [CrossRef]
11. Bansal, T.; Talakokula, V.; Sathujoda, P. A Machine Learning Approach for Predicting the Electro-Mechanical Impedance Data of Blended RC Structures Subjected to Chloride Laden Environment. *Smart Mater. Struct.* **2022**, *31*, 015036. [CrossRef]
12. Gomasa, R.; Talakokula, V.; Jyosyula, S.K.R.; Bansal, T. Integrating Electro-Mechanical Impedance Data with Machine Learning for Damage Detection and Classification of Blended Concrete Systems. *Constr. Build. Mater.* **2024**, *445*, 137725. [CrossRef]
13. Ai, D.M.; Zhang, R. Deep Learning of Electromechanical Admittance Data Augmented by Generative Adversarial Networks for Flexural Performance Evaluation of Rc Beam Structure. *Eng. Struct.* **2023**, *296*, 116891. [CrossRef]
14. Du, F.; Wu, S.; Xu, C.; Yang, Z.; Su, Z. Electromechanical Impedance Temperature Compensation and Bolt Loosening Monitoring Based on Modified Unet and Multitask Learning. *IEEE Sens. J.* **2023**, *23*, 4556–4567. [CrossRef]
15. Yang, L.J.; Yan, W. Damage Detection in a Rod Based on Direct And Inverse EMI Analysis Using the Dynamic Stiffness Matrix Method. *Arab. J. Sci. Eng.* **2026**, *51*, 21095–21107. [CrossRef]
16. Yang, L.J.; Yan, W. Modeling and Experimental Study of Cross-Electromechanical Admittance for Crack Localization in Beams with Distributed Piezoelectric Wafers. *Sensors* **2026**, *26*, 6216. [CrossRef] [PubMed]
17. Meher, U.; Sunny, M.R. Detection of Multiple Structural Damages from Drive Point and Cross Electro-Mechanical Impedance Signatures. *Mech. Adv. Mater. Struct.* **2022**, *29*, 4738–4758. [CrossRef]
18. Meher, U.; Sunny, M.R. Localization and Quantification of Delamination/Disbond Inside a Composite Lap-Joint Using Novel Cross and Drive Point Mechanical Impedance Based Feature. *Mech. Syst. Signal Process.* **2024**, *220*, 111661. [CrossRef]
19. Yang, L.J.; Yan, W.; Xuan, D. A Cross Electro-Mechanical Impedance Method Using a Distributed Piezoelectric Array for Bolt Loosening Detection. *Appl. Sci.* **2025**, *15*, 12605. [CrossRef]
20. Kaur, H.; Singla, S. Assessment of Reinforced Concrete Beam with Electro-Mechanical Impedance Technique Based on Piezoelectric Transducers. *Arab. J. Sci. Eng.* **2023**, *48*, 13449–13463. [CrossRef]
21. Ren, Y.Q.; Zhang, S.F.; Yuan, S.F.; Qiu, L. In-situ Integration and Performance Verification of Large-Scale PZT Network for Composite Aerospace Structure. *Smart Mater. Struct.* **2023**, *32*, 055010. [CrossRef]
22. Perera, R.; Gil, A.; Torres, L.; Barris, C. Diagnosis of NSM FRP Reinforcement in Concrete by Using Mixed-Effects Models and EMI Approaches. *Compos. Struct.* **2021**, *273*, 114322. [CrossRef]
23. Wang, T.; Tan, B.; Lu, M.; Zhang, Z.; Lu, G. Piezoelectric Electro-Mechanical Impedance (EMI) Based Structural Crack Monitoring. *Appl. Sci.* **2020**, *10*, 4648. [CrossRef]
24. Gao, X.; Zhang, H.; Jia, C.; Wu, J. Electro-mechanical Equivalent Impedance Model, Verification, and Application Investigation on High-Frequency Dual-Branch Parallel Structure Piezoelectric Ultrasonic Transducer for Electronic Packaging. *Measurement* **2026**, *258*, 119407. [CrossRef]
25. Huynh, T.C.; Koh, C.G.; Low, Y.M. Reference-Free Impedance-Based Crack Detection for Asymmetric Structures: Application to Tidal Turbine Blades. *J. Sound Vib.* **2025**, *618*, 119304. [CrossRef]
26. Xu, J.; Dong, J.H.; Li, H.N.; Zhang, C.W.; Ho, S.C. Looseness Monitoring of Bolted Spherical Joint Connection Using Electro-Mechanical Impedance Technique and BP Neural Networks. *Sensors* **2019**, *19*, 1906. [CrossRef] [PubMed]
27. Beroual, S.; Hrairi, M.; Yatim, N.M.; Dawood, M.S.I.S. Solar Cell Micro Crack Detection Technique Using Electromechanical Impedance and Finite Element Analysis. *Proc. Inst. Mech. Eng. Part C J. Mech. Eng. Sci.* **2024**, *238*, 3531–3548. [CrossRef]
28. Thoriya, A.; Vora, T.; Jadeja, R.; Ali, Y.A.A.; Patel, S.K. Application of Wavelet Transform Techniques for Corrosion Assessment of Embedded Rebars in RC Elements Using Electromechanical Impedance. *Measurement* **2024**, *226*, 114081. [CrossRef]
29. Perera, R.; Montes, J.; Gómez, A.; Barris, C.; Baena, M. Unsupervised Autoencoders with Features in the Electromechanical Impedance Domain for Early Damage Assessment in FRP-Strengthened Concrete Elements. *Eng. Struct.* **2024**, *315*, 118458. [CrossRef]
30. Lan, C.M.; Liu, H.H.; Zhuang, S.; Wang, J.J.; Li, W.J.; Lin, G.H. Monitoring of Crack Repair in Concrete Using Spherical Smart Aggregates Based on Electromechanical Impedance (EMI) Technique. *Smart Mater. Struct.* **2024**, *33*, 025031. [CrossRef]
31. Haq, M.; Tee, K.F.; Al-Osta, M.A.; Fasil, M. Monitoring Carbonation Curing of Concrete Structures Using Low-Cost Smart Piezoelectric Patches. *Arab. J. Sci. Eng.* **2026**, *51*, 5559–5568. [CrossRef]
32. Liu, Y.; Feng, X. Monitoring Corrosion-Induced Thickness Loss of Stainless Steel Plates Using the Electromechanical Impedance Technique. *Meas. Sci. Technol.* **2021**, *32*, 025104. [CrossRef]
33. De Castro, B.A.; Baptista, F.G.; Ciampa, F. New Imaging Algorithm for Material Damage Localisation Based on Impedance Measurements Under Noise Influence. *Measurement* **2020**, *163*, 107953. [CrossRef]
34. Singh, S.K.; Soman, R.N.; Malinowski, P.H. A Novel Multi-Damage Localization Method for Polymers and Composites Based on Electromechanical Impedance. *Mech. Syst. Signal Process.* **2024**, *216*, 111508. [CrossRef]

35. Khayatazad, M.; Loccuffer, M.; De Waele, W. Electromechanical Impedance-Based Measurements for Damage Detection and Characterization in Medium-Thick Plates. *Measurement* **2025**, *248*, 116841. [CrossRef]
36. Sapidis, G.M.; Naoum, M.C.; Papadopoulos, N.A.; Golias, E.; Karayannis, C.G.; Chalioris, C.E. A Novel Approach to Monitoring the Performance of Carbon-Fiber-Reinforced Polymer Retrofitting in Reinforced Concrete Beam–Column Joints. *Appl. Sci.* **2024**, *14*, 9173. [CrossRef]
37. Ai, D.M.; Zhou, A.Q.; Zhu, H.P. Axial-Pressure Identification of Laminated High Damping Rubber Bearings Using Electro-Mechanical Coupled Model of Bonded PZT Transducers. *Compos. Struct.* **2026**, *379*, 119958. [CrossRef]
38. Da Silva, C.J.R.; Budoya, D.E.; Baptista, F.G. Improving Impedance Measurement for Structural Health Monitoring by Setting the Appropriate Number of Excitation Signal Cycles. *IEEE Trans. Instrum. Meas.* **2024**, *73*, 6002612. [CrossRef]
39. Lu, R.; Shen, Y.; Qu, W.; Xiao, L. Health Monitoring of High-Damping Viscoelastic Materials Using Sub-Resonator Enriched Electro-Mechanical Impedance Signatures. *Smart Mater. Struct.* **2022**, *31*, 095046. [CrossRef]

Disclaimer/Publisher's Note: The statements, opinions and data contained in all publications are solely those of the individual author(s) and contributor(s) and not of MDPI and/or the editor(s). MDPI and/or the editor(s) disclaim responsibility for any injury to people or property resulting from any ideas, methods, instructions or products referred to in the content.